Probing softness of the parietal pleural surface at the micron scale

Jae Hun Kim[a,*], **James P. Butler**[a,b,c], and **Stephen H. Loring**[a]

[a]Department of Anesthesia, Critical Care and Pain Medicine, Beth Israel Deaconess Medical Center and Harvard Medical School, Boston, MA 02215, USA

[b]Molecular and Integrative Physiological Sciences, Harvard School of Public Health, 665 Huntington Avenue, Boston, MA, USA

[c]Division of Sleep Medicine, Department of Medicine, Harvard Medical School and Brigham and Women's Hospital, Boston, MA, USA

Abstract

The pleural surfaces of the chest wall and lung slide against each other, lubricated by pleural fluid. During sliding motion of soft tissues, shear induced hydrodynamic pressure deforms the surfaces, promoting uniformity of the fluid layer thickness, thereby reducing friction. To assess pleural deformability at length scales comparable to pleural fluid thickness, we measured the modulus of the parietal pleura of rat chest wall using atomic force microscopy (AFM) to indent the pleural surface with spheres (radius 2.5 µm and 5 µm). The pleura exhibited two distinct indentation responses depending on location, reflecting either homogeneous or significantly heterogeneous tissue properties. We found an elastic modulus of 0.38–0.95 kPa, lower than the values measured using flat-ended cylinders > 100 µm radii (Gouldstone et al., 2003, Journal of Applied Physiology 95, 2345–2349). Interestingly, the pleura exhibited a three-fold higher modulus when probed using 2.5 µm vs. 5 µm spherical tips at the same normalized depth, confirming depth dependent inhomogeneous elastic properties. The observed softness of the pleura supports the hypothesis that unevenness of the pleural surface on this scale is smoothed by local hydrodynamic pressure.

Keywords

Parietal pleura; AFM; Hertzian indentation; Elastohydrodynamic lubrication; Rat

1. Introduction

During respiratory motion, the pleural surfaces of the lung and chest wall slide reciprocally relative to each other. Pleural fluid facilitates this, but the nature of pleural lubrication has been controversial. Agostoni (1986) attributed the difference between pleural fluid pressure

*Corresponding author. Dr. Jae Hun Kim, 330 Brookline Ave., Dana 715, Boston, MA 02215, Tel : 617-667-5296, Fax : 617-667-1500, mbeads@hotmail.com.

Conflict of interest statement

The authors have no financial and personal relationships with other people or organizations that could inappropriately influence this investigation.

and lung surface pressure to points of contact between surfaces, suggesting boundary lubrication. This requires normal loads being partially supported by contacts at surface asperities, depending on the roughness and stiffness of the pleural surfaces. In an opposing view, Lai-Fook and Kaplowitz (1985) argued that a continuous fluid layer separates the pleural surfaces, implying elastohydrodynamic lubrication. Lai-Fook (2004) maintains that pleural liquid pressure is equal to pleural surface pressure.

In elastohydrodynamic lubrication, sliding of soft uneven surfaces generates hydrodynamic pressure which smoothes roughness and redistributes fluid from thick to thin fluid regions, promoting a more uniform fluid layer (Dowson and Jin, 1986; Lai et al., 2002; Butler et al., 1995). Computational work based on fluid dynamic models shows that the pressure distribution depends on the roughness wavelength and the elastic properties of the surface (Gouldstone et al., 2003a; Moghani et al. 2009). Microscopic studies of quick-frozen chests reveal pleural surface asperities with widths ranging from tens to hundreds of microns (Albertine et al., 1991). The degree to which these asperities are smoothed by hydrodynamic forces and thus the likelihood that elastohydrodynamic lubrication characterizes pleural tribology depends critically on the value of the elastic moduli of the pleural surfaces. Analytic and parametric studies show that the tissue softness enhances the lifting force during sliding, thus increasing the minimum fluid thickness (Butler and Loring, 2008; Skotheim and Mahadevan, 2005). Importantly, maintaining a uniform liquid thickness requires pleural deformation at length scales comparable to the fluid layer itself.

The elasticity of pleural tissues, which represents a measure of surface deformability, has been measured using indentation techniques (Lai-Fook et al., 1976; Hajji et al., 1979; Gouldstone et al., 2003b). These measurements have employed probes much larger than the pleural fluid thickness of ~8–20 µm (Lai-Fook and Kaplowitz, 1985); the elasticity of the pleural surface at length scales comparable to fluid thickness is currently unknown.

To fill this gap, we used atomic force microscopy (AFM) to probe tissue at the micron scale in a physiologic fluid environment (Drake et al., 1989). To avoid stress singularities associated with sharp AFM tips, we used 2.5 and 5 µm spherical tips to simulate in-vivo pleural deformations. Tissue elastic properties were determined from the AFM force/ deflection data by fitting with Hertz's elastic model of homogeneous materials (Hertz, 1882). The effect of sphere size on the probed stiffness was interpreted on the basis of structural inhomogeneity of the pleura and subjacent tissue.

We found:

1. The elastic modulus of the parietal pleura measured at the micron scale was two-fold to five-fold lower than the values previously obtained with flat probes of radii >100 µm (Gouldstone et al., 2003b).

2. There were two characteristic indentation responses, Hertzian and non-Hertzian, respectively reflecting homogeneous tissue properties and structural inhomogeneities.

2. Materials and methods

Tissue preparation

We used thirteen Sprague-Dawley rats (300 – 500g) under a protocol approved by the Institutional Animal Care and Use Committee of Beth Israel Deaconess Medical Center. Each animal received heparin (5000 units i.p.), to prevent fibrin formation on the mesothelial surface, and was killed ~ 5 min later with an overdose of sodium pentobarbital (>200mg/kg i.p.) (Lin et al. 2008). Immediately after death, the thoracic cavity was opened

and the intercostal muscles and intervening ribs were excised en bloc (~4×4×2mm) between the 3rd and 7th rib. To prevent abrasion, we avoided touching the parietal surfaces, and immersed the specimen in saline.

Atomic force microscopy

A commercial AFM (MFP-3D; Asylum, Santa Barbara, CA) was used with probes constructed with borosilicate spherical tips, nominal radius 2.5 and 5 µm, glued to triangular cantilevers with a nominal spring constant k =0.06 N/m (Novascan Technologies, Ames, Iowa). k was independently measured by the thermal noise method (Hutter and Bechhoefer, 1993; Butt and Jaschke, 1995; Stark et al., 2001). The laser detector was calibrated for zero force before each experiment. The piezotranslator extended and retracted the probe at 2 µm/ s. Measurements were completed within 5h after death. One specimen from each rat was used for these measurements. Ten to 100 force-displacement curves were collected from each rat, separated laterally by at least 5 and 10 µm for 2.5 and 5 µm tips, respectively. Maximum forces were ~4nN.

Data analysis

From Hooke's law, force F is linearly related to deflection, $F = kd$, where d is the deflection of the cantilever. The indentation depth δ is the relative displacement of cantilever holder ($z - z_c$) minus d, where z is the displacement of the piezo actuator and z_c is the contact point. The classical Hertz model for homogeneous material describes the force/depth relation for spherical punch indentations. For incompressible tissue and a probe of radius R, this relation is

$$F = \frac{16ER^{1/2}}{9}\delta^{3/2} = \frac{16E}{9}a\delta \tag{1}$$

where E is Young's modulus, and a is the radius of contact between the punch and the surface (Hertz, 1882). In terms of z and d,

$$z - d - z_c = \left(\frac{9}{16ER^{1/2}}\right)^{2/3} F^{2/3} \tag{2}$$

From direct measurements of z and d, E can be extracted from Eq. 2 if z_c can be found. Determination of z_c is nontrivial for soft tissues, because the initial deflection is small and nonlinear (Crick and Yin, 2007), and force-depth curves often do not show a clear transition when tip-tissue contact is made. We used least squares fitting rather than visual inspection or other methods for determining z_c and E (Lin and Horkay, 2008; Shoelson et al, 2004). Much of our data showed weak force increases over large depths, followed by progressive steepening, which we attributed to surface heterogeneity (Fig. 2b). To robustly detect initial force increase, we performed initial fitting in a small force window for the first guess of contact point, and searched iteratively for the best z_c. The left panel of Fig. 1 shows typical force-displacement data from approach (loading) and retraction (unloading). During retraction, negative and discontinuous forces were observed, a pattern characteristic of adhesion between the tip and the underlying tissue (Wojcikiewicz et al., 2003; Sen et al., 2005). This was not seen in the approaching phase, suggesting negligible adhesion artifacts. We therefore analyzed only approach curves. Initially, F *vs.* z data were fitted to the Hertz model over a range of forces from 0.2 to 0.8 nN, the latter approximating 20% of the maximum force at maximal indentation. The intersection between the fitted curve and the zero force line was picked as an initial guess of z_c. The force-displacement data were then

fitted to the Hertz model over a range of depths (depth window) in the post-contact region and to zero force in the pre-contact region. z_c was then varied in 4 nm increments between 0.4–0.8 µm below and above the initial guess. The root mean squared error (RMS) was computed for each z_c guess, and the value of z_c that minimized the RMS was taken as the contact point (right panel of Fig. 1). E was recovered from Eq. 2, here referred to as overall stiffness E_o. Force and depth windows and sweep ranges of contact points for each probe are summarized in Table 1. By setting maximum normalized depths of the fitting windows equal, we ensured that the average strain was the same for all probes (see Appendix A).

After contact point analysis, the mean squared depth-wise error over the whole range of F vs. z data (RMS$_{whole}$) was computed for each curve, as an index of deviation from the homogeneous elastic model. Average E_o for each rat was determined after excluding the 10% of indentation curves with the highest RMS$_{whole}$. The averages from 10 rats for each probe were compared using unpaired two-tailed Student's t-tests. In addition to E_o, E was computed at each data point according to Eq. 2, giving an apparent pointwise stiffness E_p at each indentation depth (Costa and Yin, 1999). Finally, the high force stiffness E_{hf} was computed over a force window (2–4 nN) (Domke and Radmacher, 1998) directly from the F vs. z curves, fitted to Eq. 2 without constraining z_c.

3. Results

Fig. 2 shows representative F vs. δ curves and the dependence of E_p on indentation depth. The pleural surfaces exhibited two distinct responses, Hertzian (consistent with homogeneous tissue properties) and non-Hertzian (indicating significant departures from elastic homogeneity). Most fitted the Hertz model with good agreement (left panel), but a few deviated widely (right panel). Most of the Hertzian curves showed a plateau of E_p as in Fig. 2c, suggesting minimal effect of tissue nonlinearity or inhomogeneity. On the other hand, many non-Hertzian curves showed a low initial slope, progressively steepening at greater penetrations, as in Figs. 2b and 2d. This depth dependent increase of stiffness implies either nonlinearities or inhomogeneities in the tissue properties. To the extent that strains are relatively small, nonlinearities are negligible, and departures from Hertzian behavior are likely due to structural inhomogeneities. Furthermore, the slope of the curve at depths beyond the fitting window in Fig. 2b is similar to that seen in Fig. 2a. These two characteristic responses were distinguished by computing RMS$_{whole}$. In Table 2, E_o and E_{hf} are compared between the 10% of curves with the highest RMS$_{whole}$ and the remainder. The stiffness of the groups is substantially different when computed over small depth windows (p=0.007, unpaired two-tailed Student's t test), but not different when measured at high force or large depth. This dependence on probing depth is clearly depicted in the left panel of Fig. 3 showing the distribution of RMS$_{whole}$ plotted against E_o and E_{hf}. This plot shows that most of indentation curves with high RMS$_{whole}$ exhibit unusually low E_o, but normally high E_{hf}. The right panel of Fig. 3 shows the distinct distributions of E_o and E_{hf}. Although the population of non-Hertzian responses was variable among individuals, the 90% subset with low RMS$_{whole}$ taken as the average (Table 3) is not statistically different among individuals.

Table 3 summarizes the results of AFM measurement on parietal pleural stiffness. Overall stiffness (E_o) is relatively consistent for a given probe size, but differs three-fold between 2.5 and 5 µm probes, the latter being lower (unpaired two-tailed Student's t test, p<0.01). There is clearly a probe size dependence of stiffness.

4. Discussion

Two characteristic indentation responses

We observed mostly Hertizan responses and fewer non-Hertzian responses for each rat, and found less variation in mechanical properties with deeper probing compared to shallow probing (Table 2). Mesothelial surfaces are typically covered with several components that could affect the surface stiffness. For example, microvilli, 1–2 µm long brush-like protrusions could support a load through a repulsive reaction between fibers similar to a polymeric brush (de Gennes, 1987; Butt et al., 1999; Sokolov et al., 2007). Glycocalyx or hyaluronic acid remaining on microvilli could cause a small initial indentation force prior to contact with deeper tissue. Fig. 4 shows cross sections of the pleura with components of microvilli, mesothelial cells, a basal membrane, elastic fibers and collagen bundles. The left panel of Fig. 4 depicts the parietal pleura covered with a thin flat mesothelial cell, of several microns thickness, comparable to the maximum indentation depth in the contact point analysis for E_o. We speculate that if the parietal pleura probed in the current study was covered with thin flat mesothelial cells covered with microvilli, the superficial indentation measurement would be sensitive to their existence. Although this would contribute to the curve fitted estimate of z_c, we note that the apparent indentation modulus through fitting is a good measure of deformability under micron sized contact area/indentation depths, and that this reflects the actual scale of deformation of the pleura during sliding. On the other hand, deeper indentation would be dominated by the stiffness of the cells or other submesothelial components. As the depth increases, so too does the lateral spatial extent contributing to the stiffness; this effective spatial averaging would then lead to relative homogeneity of behavior at these higher indentation depths, consistent with our observations.

Tip size dependence of stiffness

The size effect may also reflect a superficial membrane of the pleura, supporting tension and affecting indentation measurements (Hajji et al., 1979). In the current study the tissue was relieved of pre-stress by excision, but we note that indentations induce in-plane stretch, in turn generating membrane tension. Membrane contributions depend on the stretch and curvature (i.e. probe size), so micro-sized indentations would be significantly altered by a slight increase of the local tension. We tested the effect of the local membrane tension using finite element (FE) simulations previously developed for a pre-tension study (Kim and Gouldstone, 2008). Table 4 shows that simplified FE models with a stiff membrane on the surface exhibit indentation stiffness twice that of the elastic solid with an increase of local membrane tension much less than that found in intact lung or chest wall (Table 5). Our model mimicked ~ 15% difference of stiffness between probe sizes, but did not predict larger differences even with higher membrane tension.

Surface roughness may also contribute to probe size dependence. We recently measured the surface topography of the parietal pleura using electron microscopy and AFM (Kim et al., 2011). We found that there is small scale vertical surface roughness on the order of 10 µm or less that could affect our measurement. Quantitatively, the Hertz relation predicts a 13~27% difference in apparent modulus between two probes (radius R and $2R$) for the effective radius of curvature of the surface $R_{surface} = 0.1R \sim 2R$, which is the upper limit of the roughness effect at shallow indentation ($a \leq R_{surface}$) (see Appendix B). We note that this is smaller than our findings of a 3 fold difference in modulus between 2.5 and 5 µm probes.

Comparison with other probes and critique of method

The range of stiffness measured using our micron-scaled probes was two-fold to five-fold lower than values previously reported using larger probes (Gouldstone et al., 2003b). Table 5 summarizes these comparisons. Origins of these differences include the following: (1)

Probing at greater strains leads to nonlinearities and increased apparent stiffness (Dimitriadis et al., 2002). In general, our choice of maximum normalized depth is less than a half of those in previous studies. We tested this potential contribution of nonlinearity at greater depths by increasing the maximum normalized depth of 2.5 µm spheres (δ_{max} / a) from 0.56 to 0.8. This deeper probing increased the average stiffness less than 20%, far less than the difference between the current and previous measurements. (2) A pre-tensed membrane increases the apparent stiffness. For example, the pleural membrane contributed 30% to the indentation force for dog lungs inflated at 4 cm H_2O (Hajji et al., 1979). But as noted above, excision itself of the tissue b locks tends to minimize membrane pre-stress. (3) The stiffness of the chest cage in Table 5 may reflect the effect of pre-strain in tissues. However, Gouldstone et al. (2003b) reported this to be negligible at low strains. Note that lung shear modulus, which varies linearly with inflation pressure at all but high lung volumes, is similar at low lung volumes to that of the parietal pleural surface in the current study. (4) The stiffness of the lung epithelial cell measured at the micron scale is two-fold higher than the parietal pleural surface; this is consistent with a higher stiffness being found with sharp probes compared to spherical probes (Rico et al., 2005; Shoelson et al. 2004), suggesting the two respiratory tissues have a similar stiffness at small scales. (5) Loading conditions, e.g. timing and velocity, may affect indentation stiffness due to stress-relaxation and squeeze-out of interstitial fluid from the region under the probe. We used triangular displacement wave-forms with constant velocity of 2 µm/s; the estimated strain rate was similar to those in previous studies in Table 5.

In this work, our analysis was based on the assumption that the material properties were probed in a quasi-static manner; we did not include time-dependent behavior. We did observe a slight difference between the approach and retraction phases (Fig. 1a). This hysteresis is characteristic of dissipative behavior (Duszyk et al., 1989), an effect which has been extensively emphasized in tissue studies (Moreno-Flores et al., 2010; Lenormand et al., 2004). To quantify the possible effect of dissipation in the on and off ramp transients of our experiments, we converted the hysteresis area of force-displacement curves, obtained using a flat punch of 0.9 µm radius at 2µm/sec velocity, to phase lag θ in the frequency domain and estimated the dissipative effect using the power law structural damping model (Hildebrandt, 1970, see Appendix C). For our pleural tissue samples, we found a power-law exponent of $\alpha = 0.052 \pm 0.042$ (21 indentation curves), which is very small compared to exponents of 0.2 ~ 0.3 found in many cell types (Alcaraz et al., 2003; Lenormand et al., 2004; Puig-De-Morales et al., 2001). Importantly, this finding predicts that a frequency increase over a decade would increase the storage modulus by only ~5%. Furthermore, the error associated with neglecting dissipative effect in our protocol would be at most less than 10%. Our preliminary data showed that E_o varied less than 10% within velocity ranges of 1–6 µm/s, consistent with the prediction above.

We assumed that deformations analyzed with Eq. 1 were small. The Hertz model is most accurate when the average strain a/R < 10% (Yoffe, 1984), but it has been used at larger strains in many cases of soft tissue or cell measurement (Gouldstone et al., 2003b; Rico et al., 2005; Rosenbluth et al., 2006). Our FE analysis shows errors of less than 10% even for a/R ~ 60%, which is small compared with variations of stiffness observed among rats or locations within a sample. Unfortunately, shallow indentations require better resolution in force and depth, and the fluid environment introduces noise making such measurements problematic with soft tissues.

Stiffness of parietal pleura and lubrication mechanism

The low stiffness of the pleura at the micron scale found in the current study has implications for respiratory lubrication mechanisms. The shear strain required to match the shape of the lung to that of the chest has been estimated to be on the order of 10% (Loring et

al., 2005). The pleural pressure varies locally according to the height in the pleural space and geometries of conformation between the chest wall and the lung. The spatial variations in pleural pressure with normal breathing (~ 1 kPa; Agostoni, 1986) are consistent with the pressures required to achieve deformation and conformation of the opposing pleural surfaces. On the other hand, relatively homogeneous pleural liquid thickness observed over wide regions of the pleural space (Lai-Fook and Kaplowitz, 1985) implies that spatial variation in normal stress is borne either by a continuous fluid layer or by tissue-tissue contact at a few asperities. The softness of the pleural surfaces found in the current study suggests that asperities are unable to support the observed pressure variations. These observations also support the idea that pleural lubrication is elastohydrodynamic. The softness of the pleural surface at this length scale promotes smoothing and conformation of the surfaces, and promotes spatial uniformity of the lubricating layer thickness. This reduces local shear stresses to approximately 10~20 Pa during resting ventilation (D'angelo et al. 2004; Loring et al., 2005), levels that are protective against tissue damage.

4. Conclusion

We studied the mechanical properties of the parietal pleura using micron-sized probes, finding stiffness two- to five-fold lower than that found with larger probes. The relative consistency of tangent stiffness at greater depths of penetration suggests that tissues share similar elastic mechanical responses at larger length scales.

We conclude that the softness of the pleura leads to tissue deformation promoting uniformity of fluid thickness and elastohydrodynamic lubrication, reducing friction during breathing.

Acknowledgments

Appendix A

To determine the maximum depth range of fitting for each probe, we computed an average strain. From Eq. 1, an average strain becomes

$$\frac{F}{\pi a^2} = C\frac{a}{R} = C\frac{\delta}{a}, \text{spherical punch,} \tag{A1}$$

where $C = 16E/9\pi$ is the incompressible stiffness constant, $F/\pi a^2$ is the average pressure applied by the punch, and δ / a is the normalized depth representing average strain. Following the same approach:

$$\frac{F}{\pi a^2} = C\frac{3\delta}{2a}, \text{flat−ended punch,} \tag{A2}$$

$$\frac{F}{\pi a^2} = C\frac{3\pi^2\delta}{16a}, \text{uniform pressure punch,} \tag{A3}$$

where $3\delta/2a$ and $3\pi^2\delta/16a$ are the respective normalized depths representing average strain (Sneddon, 1946; Johnson, 1985). Eqs. A1, A2 and A3 compare average strains of three probe geometries for given indentation depths and radii.

Appendix B

In Eq. 1, if the surface is curved, the apparent modulus E_{app} will be dependent on a relative radius of curvature R^*:

$$F=E\frac{16\delta^{3/2}R^{*1/2}}{9}=E_{app}\frac{16\delta^{3/2}R^{1/2}}{9}, R^*=\frac{R\times R_{surface}}{R+R_{surface}}$$
(B1)

where R is the radius of a spherical probe and $R_{surface}$ is the radius of curvature of the surface (Johnson, 1985). From this it follows that

$$E_{app}=E\left(\frac{R_{surface}}{R+R_{surface}}\right)^{1/2}$$
(B2)

If we define a roughness parameter $\chi=R_{surface}/R$, then the ratio between two apparent moduli is

$$\frac{E_{app,2R}}{E_{app,R}}=\left(\frac{1+\chi}{2+\chi}\right)^{1/2}$$
(B3)

where $E_{app,R}$, and $E_{app,2R}$ are apparent moduli for two probes with radii R and $2R$, respectively.

Appendix C

The area of a hysteresis loop is related to hysteresivity η and phase lag θ regardless of linearity of the system via the following relations:

$$\eta=\tan(\theta)$$
(C1)

$$\theta=\sin^{-1}(4\Delta A/\pi A)$$
(C2)

where A is the total area of a rectangular box bounding the loop, and ΔA is the hysteresis loop area (Fredberg and Stamenovic, 1989). In the power law model, the complex modulus is defined as

$$E^*(\omega)=E_s(1+i\eta)\left(\omega/\omega_s\right)^\alpha$$
(C3)

where E_s is a scale factor for modulus, ω_s is a scale factor for frequency and $\alpha=2\theta/\pi$ is the power-law exponent (Fabry et al., 2001).

References

Agostoni, E. Handbook of Physiology. The Respiratory System. Mechanics of Breathing. Vol. vol. III. Bethesda, MD: American Physiology Society; 1986. Mechanics of the pleural space; p. 531-559.sect. 3
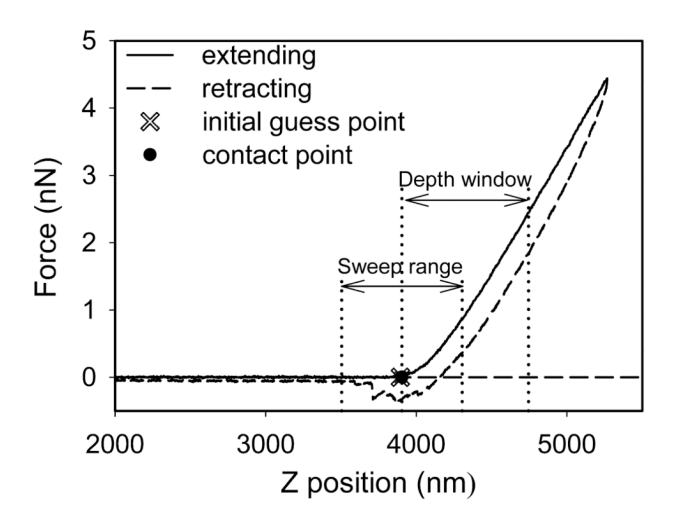
Albertine KH, Wiener-Kronish JP, Bastacky J, Staub NC. No evidence for mesothelial cell contact across the costal pleural space of sheep. Journal of Applied Physiology. 1991; 70:123–134. [PubMed: 2010367]

Alcaraz J, Buscemi L, Grabulosa M, Trepat X, Fabry B, Farre R, Navajas D. Microrheology of human lung epithelial cells measured by atomic force microscopy. Biophysical Journal. 2003; 84:2071–2079. [PubMed: 12609908]

Butler JP, Huang J, Loring SH, Lai-Fook SJ, Wang PM, Wilson TA. Model for a pump that drives circulation of pleural fluid. Journal of Applied Physiology. 1995; 78:23–29. [PubMed: 7713817]

Butler JP, Loring SH. A potential elastohydrodynamic origin of load-support and coulomb-like friction in lung/chest wall lubrication. Journal of Tribology-Transactions of the ASME. 2008; 130:141201.1–141201.7.

Butt HJ, Jaschke M. Calculation of thermal noise in atomic-force microscopy. Nanotechnology. 1995; 6:1–7.

Butt HJ, Kappl M, Mueller H, Raiteri R, Meyer W, Ruhe J. Steric forces measured with the atomic force microscope at various temperatures. Langmuir. 1999; 15:2559–2565.

Costa KD, Yin FDP. Analysis of indentation: Implications for measuring mechanical properties with atomic force microscopy. Journal of Biomechanical Engineering-Transactions of the ASME. 1999; 121:462–471.

Crick SL, Yin FCP. Assessing micromechanical properties of cells with atomic force microscopy: importance of the contact point. Biomechanics and Modeling in Mechanobiology. 2007; 6:199–210. [PubMed: 16775736]

D'Angelo E, Loring SH, Gioia ME, Pecchiari M, Moscheni C. Friction and lubrication of pleural tissues. Respiratory Physiology and Neurobiology. 2004; 142:55–68. [PubMed: 15351304]

de Gennes PG. Polymers at an interface - a simplified view. Advances in Colloid and Interface Science. 1987; 27:189–209.

Dimitriadis EK, Horkay F, Maresca J, Kachar B, Chadwick RS. Determination of elastic moduli of thin layers of soft material using the atomic force microscope. Biophysical Journal. 2002; 82:2798–2810. [PubMed: 11964265]

Domke J, Radmacher M. Measuring the elastic properties of thin polymer films with the atomic force microscope. Langmuir. 1998; 14:3320–3325.

Dowson D, Jin ZM. Micro-elastohydrodynamic lubrication of synovial joints. Engineering in Medicine. 1986; 15:63–65. [PubMed: 3709914]

Drake B, Prater CB, Weisenhorn AL, Gould SAC, Albrecht TR, Quate CF, Cannell DS, Hansma HG, Hansma PK. Imaging Crystals, Polymers, and Processes in Water with the Atomic Force Microscope. Science. 1989; 243:1586–1589. [PubMed: 2928794]

Duszyka M, Schwab B, Zahalaka GI, Qiana H, Elsona EL. Cell poking - quantitative-analysis of indentation of thick viscoelastic layers. Biophysical Journal. 1989; 55:683–690. [PubMed: 2720066]

Fabry B, Maksym GN, Butler JP, Glogauer M, Navajas D, Fredberg JJ. Scaling the microrheology of living cells. Physical Review Letters. 2001; 87:148102.1–148102.4. [PubMed: 11580676]

Fredberg JJ, Stamenovic D. On the imperfect elasticity of lung tissue. Journal of Applied Physiology. 1989; 67:2408–2419. [PubMed: 2606848]

Gouldstone A, Brown RE, Butler JP, Loring SH. Elastohydrodynamic separation of pleural surfaces during breathing. Respiratory Physiology and Neurobiology. 2003a; 137:97–106. [PubMed: 12871681]

Gouldstone A, Brown RE, Butler JP, Loring SH. Stiffness of the pleural surface of the chest wall is similar to that of the lung. Journal of Applied Physiology. 2003b; 95:2345–2349. [PubMed: 14600162]

Gulliver, G. On the size and shape of red corpuscles of the blood of vertebrates, with drawings of them to a uniform scale, and extended and revised tables of measurements; Proceedings of the Royal Society of London; 1875. p. 474-495.

Hajji MA, Wilson TA, Lai-Fook SJ. Improved measurements of shear modulus and pleural membrane tension of the lung. Journal of Applied Physiology. 1979; 47:175–181. [PubMed: 468657]

Hertz H. Über die Berührung fester elastischer Körper (On the contact of elastic solids). Journal fur die Reine und Angewandte Mathematik. 1882; 92:156–171.

Hildebrandt J. Pressure-volume data of cat lung interpreted by a plastoelastic, linear viscoelastic model. Journal of Applied Physiology. 1970; 28:365–372. [PubMed: 5414773]

Hutter JL, Bechhoefer J. Calibration of atomic-force microscope tips. Review of Scientific Instruments. 1993; 64:1868–1873.

Johnson, KL. Contact mechanics. Cambridge: Cambridge University Press; 1985. p. 90-104.

Kim JH, Butler JP, Loring SH. Influence of the softness of the parietal pleura on respiratory sliding mechanisms. Respiratory Physiology and Neurobiology. 2011; 177:114–119. [PubMed: 21473935]

Kim JH, Gouldstone A. Spherical indentation of a membrane on an elastic half-space. Journal of Materials Research. 2008; 23:2212–2220.

Lai J, Gouldstone A, Butler JP, Federspiel WJ, Loring SH. Relative motion of lung and chest wall promotes uniform pleural space thickness. Respiratory Physiology and Neurobiology. 2002; 131:233–243. [PubMed: 12126924]

Lai-Fook SJ. Pleural mechanics and fluid exchange. Physiological Reviews. 2004; 84:385–410. [PubMed: 15044678]

Lai-Fook SJ, Kaplowitz MR. Pleural space thickness in situ by light microscopy in five mammalian species. Journal of Applied Physiology. 1985; 59:603–610. [PubMed: 4030613]

Lai-Fook SJ, Wilson TA, Hyatt RE, Rodarte JR. Elastic constants of inflated lobes of dog lungs. Journal of Applied Physiology. 1976; 40:508–513. [PubMed: 931871]

Lenormand G, Millet E, Fabry B, Butler JP, Fredberg JJ. Linearity and time-scale invariance of the creep function in living cells. Journal of the Royal Society. 2004; 1:91–97.

Lin DC, Horkay F. Nanomechanics of polymer gels and biological tissues: A critical review of analytical approaches in the Hertzian regime and beyond. Soft Matter. 2008; 4:669–682.

Lin JL, Moghani T, Fabry B, Butler JP, Loring SH. Hydrodynamic thickening of lubricating fluid layer beneath sliding mesothelial tissues. Journal of Biomechanics. 2008; 41:1197–1205. [PubMed: 18367193]

Loring SH, Brown RE, Gouldstone A, Butler JP. Lubrication regimes in mesothelial sliding. Journal of Biomechanics. 2005; 38:2390–2396. [PubMed: 16214486]

Michailova KN. Electron microscopic alterations of the rat's pleura after experimental haemothorax. Annals of Anatomy-Anatomischer Anzeiger. 2004; 186:115–125.

Moghani T, Butler JP, Loring SH. Determinants of friction in soft elastohydrodynamic lubrication. Journal of Biomechanics. 2009; 42:1069–1074. [PubMed: 19358993]

Moreno-Flores S, Benitez R, Vivanco MD, Toca-Herrera JL. Stress relaxation microscopy: imaging local stress in cells. Journal of Biomechanics. 2010; 43:349–354. [PubMed: 19772964]

Puig-De-Morales M, Grabulosa M, Alcaraz J, Mullol J, Maksym GN, Fredberg JJ, Navajas D. Measurement of cell microrheology by magnetic twisting cytometry with frequency domain demodulation. Journal of Applied Physiology. 2001; 91:1152–1159. [PubMed: 11509510]

Rico F, Roca-Cusachs P, Gavara N, Farre R, Rotger M, Navajas D. Probing mechanical properties of living cells by atomic force microscopy with blunted pyramidal cantilever tips. Physical Review E. 2005; 72:021914.1–021914.10.

Rosenbluth MJ, Lam WA, Fletcher DA. Force microscopy of nonadherent cells: A comparison of leukemia cell deformability. Biophysical Journal. 2006; 90:2994–3003. [PubMed: 16443660]

Sen S, Subramanian S, Discher DE. Indentation and adhesive probing of a cell membrane with AFM: Theoretical model and experiments. Biophysical Journal. 2005; 89:3203–3213. [PubMed: 16113121]

Shoelson B, Dimitriadis EK, Cai HX, Kachar B, Chadwick RS. Evidence and implications of inhomogeneity in tectorial membrane elasticity. Biophysical Journal. 2004; 87:2768–2777. [PubMed: 15454468]

Skotheim JM, Mahadevan L. Soft lubrication: The elastohydrodynamics of nonconforming and conforming contacts. Physics of Fluids. 2005; 17:092101.1–092101.23.

Sneddon IN. Boussinesq's problem for a flat-ended cylinder. Proceedings of the Cambridge Philosophical Society. 1946; 42:29–39.

Sokolov I, Iyer S, Subba-Rao V, Gaikwad RM, Woodworth CD. Detection of surface brush on biological cells in vitro with atomic force microscopy. Applied Physics Letters. 2007; 91:023902.1–023902.3.

Stark RW, Drobek T, Heckl WM. Thermomechanical noise of a free v-shaped cantilever for atomic-force microscopy. Ultramicroscopy. 2001; 86:207–215. [PubMed: 11215624]

Yoffe, EH. Philosophical Magazine A-Physics of Condensed Matter Structure Defects and Mechanical Properties. Vol. 50. 1984. Modified Hertz theory for spherical indentation; p. 813-828.

Wojcikiewicz EP, Zhang X, Chen A, Moy VT. Contributions of molecular binding events and cellular compliance to the modulation of leukocyte adhesion. Journal of Cell Science. 2003; 116:2531–2539. [PubMed: 12734401]
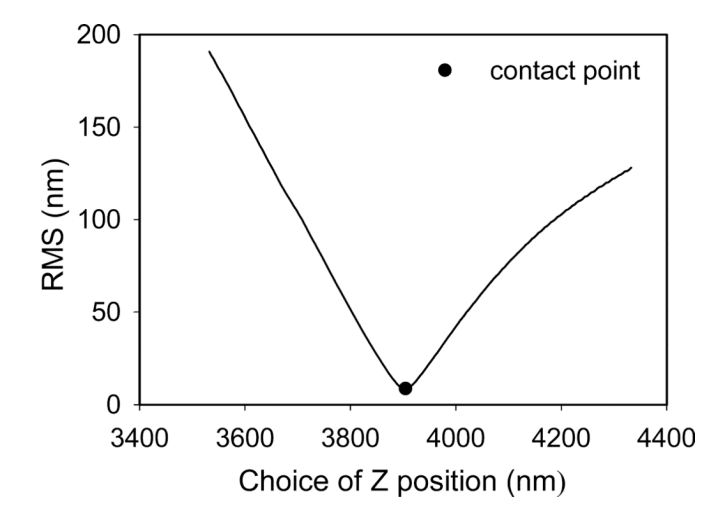
Fig. 1.
Typical AFM data and root mean square error (RMS) plot. Left: a representative force-displacement curve, showing depth window, sweep range and initial contact point marked as dotted lines and a dot, respectively. Right: RMS error for the curve to the left as a function of the choice of contact point (z). Indentation was performed with a 2.5 µm sphere in saline.
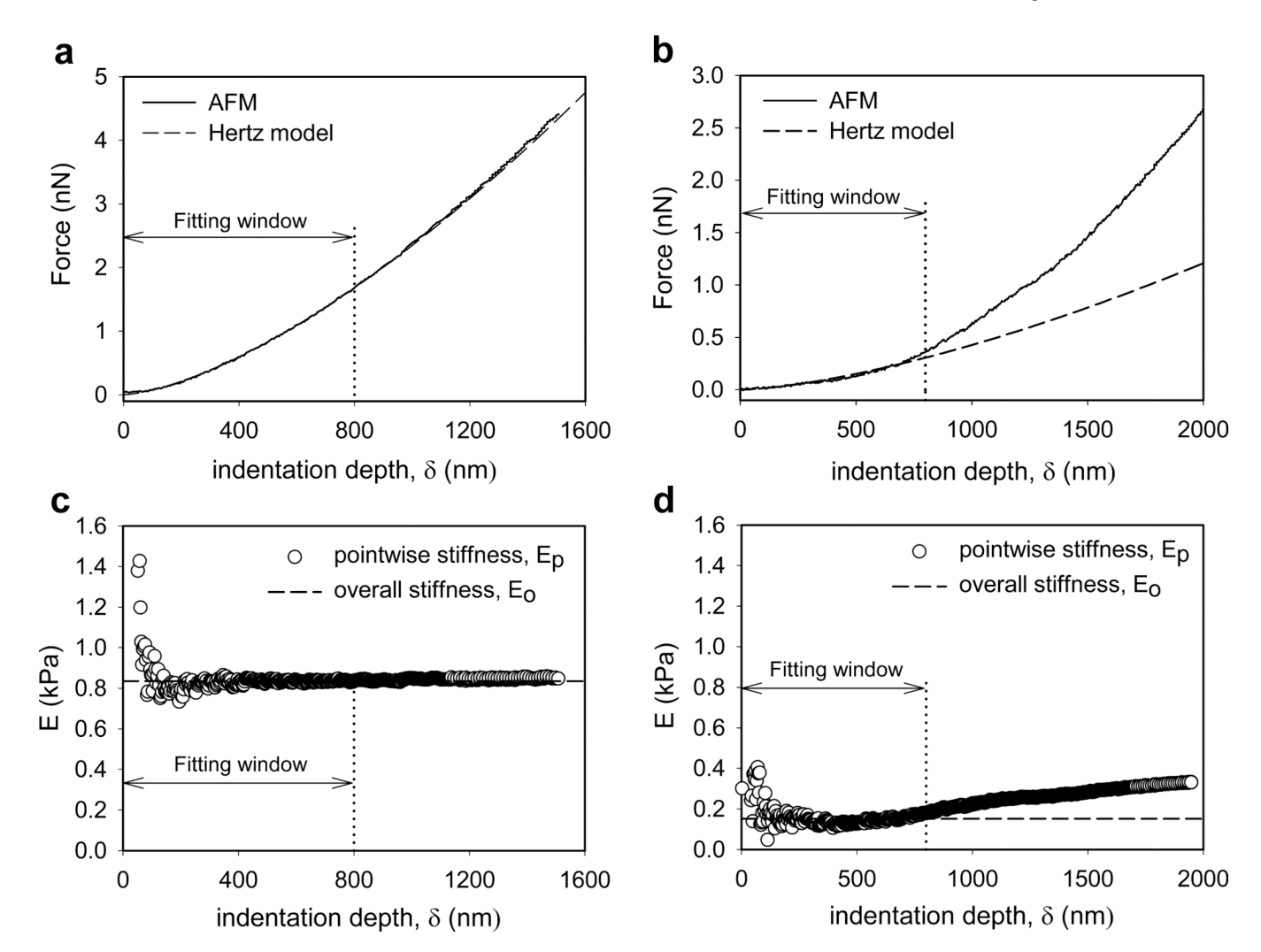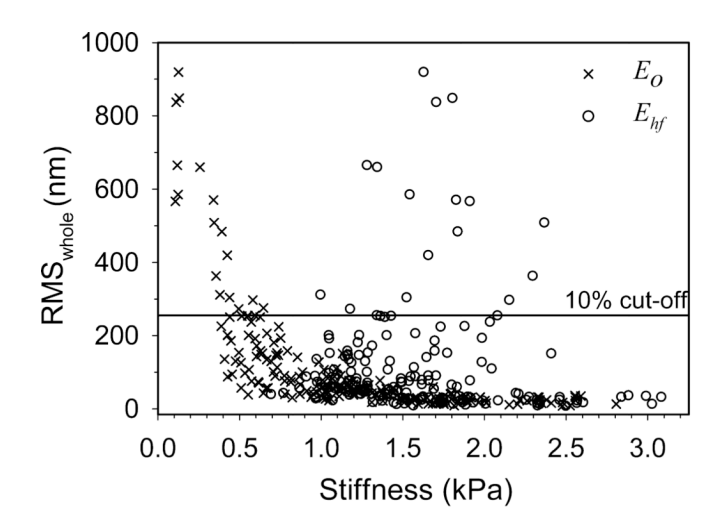
Fig. 2.
Representative *F vs.* δ curves and dependence of stiffness on depth[*]. Examples showing good agreement with the Hertz model (a) and large deviation from the elastic model (b), see text. Pointwise stiffness E_p as a function of indentation depth and overall stiffness E_o (dashed line) are shown in c, d for curves in a, b. Depth windows for fitting are marked as vertical dotted lines. Indentations were performed with a 2.5 µm sphere in saline. * Data was obtained from rat S1. Rats used for stiffness measurements are listed in Table 3.
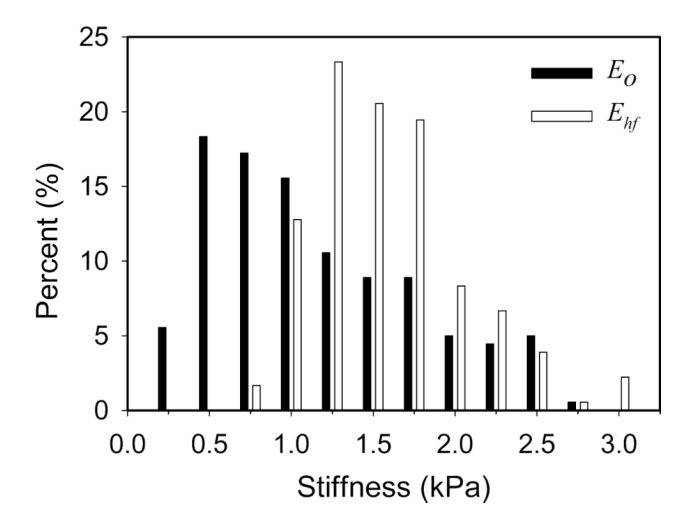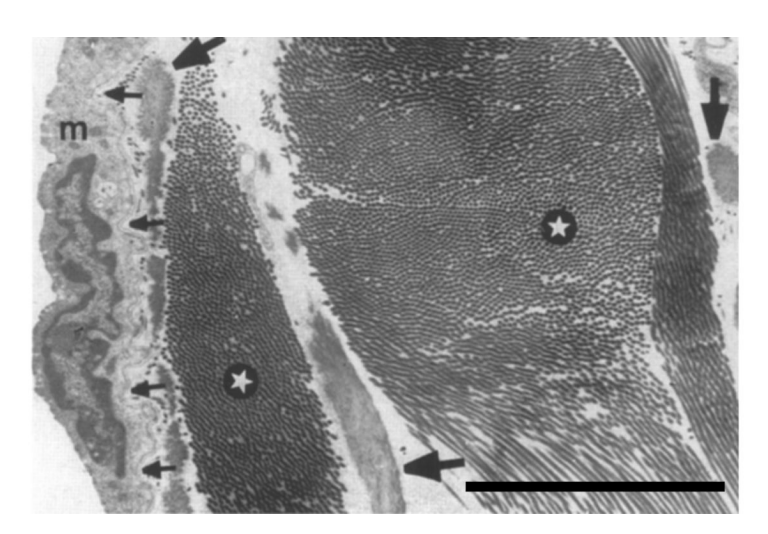
Fig. 3.
Histograms of stiffness from S1. Left: Plots of RMS_{whole} versus overall stiffness E_o (X) and high force stiffness E_{hf} (open circle). Right: Distribution of overall stiffness E_o (black) and high force stiffness E_{hf} (white). Average E_o calculation excludes 10% of data with the highest RMS_{whole} (horizontal line).
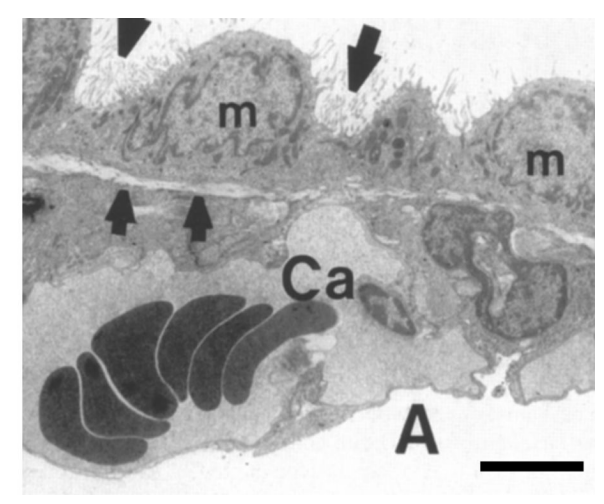
Fig. 4.
Cross sectional images of the pleurae of Wistar rat. Left: Parietal pleura. Flat mesothelial cell (m), basal lamina (small arrows), collagen bundles (asterisk) and elastic fibers (large arrow) are marked. Right: Visceral pleura. Microvilli (large arrows), cubical mesothelial cells (m), elastic membrane (small arrows), peripheral blood capillary (Ca) and alveolus (A) are marked. Scale bars (5 µm) are estimated by comparing the erythrocyte diameter observed in the right panel to the reported value for rat (Gulliver, 1875). Images modified from Michailova (2004, Copyright Elsevier).

Table 1

Summary of fitting parameters used for determining contact point and stiffness.

	2.5 µm sphere	5 µm sphere
Force window for initial guess of contact point	0.2–0.8 nN	0.2–0.8 nN
Depth window ($z - z_c - d$)	0.8 µm	1.6 µm
Sweep range of contact point (left/right)	0.4/0.4 µm	0.8/0.8 µm
Maximum normalized depth ($\delta_{max} / a_{max} = a_{max} / R$)	0.56	0.56

Table 2

Comparison of overall stiffness (E_o) and high force stiffness (E_{hf}) between groups with highest (10%) and low (90%) RMS$_{whole}$.

Rat[*]	N[**]	Overall stiffness (E_o, kPa)[†]		High force stiffness (E_{hf}, kPa)	
		10%[††]	90%	10%	90%
S1	180	0.33 ±0.18	1.24 ±0.60	1.78 ±0.60	1.58 ±0.48
S3	71	0.11 ±0.03	0.87 ±0.63	1.33 ±0.36	1.44 ±0.62
S4	82	0.13 ±0.05	0.79 ±0.50	0.86 ±0.39	1.09 ±0.55

[*] Only the data with 2.5 μm sphere are analyzed for the high force stiffness to avoid the complication of the probe size effect (see Table 3), and only those rats with > 50 indentations are presented here.

[**] Total number of indentation curves analyzed for each rat.

[†] E_O was extracted from contact point analysis in small depth window (0–0.8 μm) and E_{hf} was computed in high force window (2–4 nN), which is interpreted as a piecewise cord slope of F vs. z curve at high force or large penetration.

[††] Averaged over the 10% of the indentation curves with the highest RMS$_{whole}$ and the rest of 90% for each rat, representing the non-Hertzian group and the Hertzian group, respectively. Overall stiffness values are statistically different (p=0.007) but high force stiffness values are similar between two groups (p=0.89).

Table 3

Stiffness (E_o) of mesothelial surface measured using spherical probes.

Probe	Rat	n*	Average stiffness ±SD (kPa)	Mean of stiffness for probe (kPa) **
2.5 µm sphere	S1	162	1.24 ±0.60	0.95 ±0.22
	S2	19	1.13 ±0.43	
	S3	64	0.87 ±0.63	
	S4	74	0.79 ±0.50	
	S5	21	0.73 ±0.44	
5 µm sphere	S6	96	0.55 ±0.15	0.38 ±0.11
	S7	113	0.38 ±0.14	
	S8	18	0.28 ±0.14	
	S9	18	0.41 ±0.09	
	S10	13	0.30 ±0.10	

*
Number of 90% of the indentation curves with low RMS_{whole}.

**
Stiffness values for 5 µm sphere are statistically lower than those for 2.5 µm sphere (p=0.0006).

Table 4

Results of FE modeling with a stiff membrane on elastic solid exhibiting probe size dependence of indentation stiffness.

Input stiffness (membrane/solid) (kPa)[*]	−/0.5	200/0.5	200/0.5
Maximum local tension (N/m)[**]	0	3.55×10^{-3}	4.1×10^{-3}
Probe radius (µm)	2.5	2.5	5
Measured stiffness (E_o) (kPa) [†]	0.51	1.32	1.12

[*] Membrane was modeled as unit thickness (1 µm) layer with zero bending stiffness.

[**] Local tension was measured at the center of the model at maximum depths of 0.8 and 1.6 µm for 2.5 and 5 µm probes, respectively. Zero tension represents elastic solid without membrane.

[†] Indentation data from FE models were analyzed using the same procedure described in method section.

Table 5

Stiffness of parietal pleura in the current study compared to previous measurements on respiratory tissues and cells

Tissue	Current study Mesothelium on intercostals muscle		Previous studies		
			Chest cage† (Pleural surface of thorax)	Lung††	Lung epithelial cell†††
Pleural membrane tension (N/m)*	-		4.9	1–15	-
Probe type and radius	2.5 µm sphere	5 µm sphere	0.01–0.1 cm cylinders	0.4–1.25 cm water columns	Sharp pyramid
Maximum normalized depth**	$0.56\ (\delta_{max}/a)$	$0.56\ (\delta_{max}/a)$	$1.5\ (3\delta_{max}/2a)$	$1.5\ (3\pi^2\delta_{max}/16a)$	$-\ (\delta_{max} \sim 0.5\ \mu m)$
Stiffness (kPa)	0.95	0.38	2	0.74–2.7	1.6

*
The pleural membrane was pre-tensed in the previous experiments of chest cage and lung.

**
Normalized depth represents average strain for each probe (see Appendix A).

†
Intact chest walls of dogs, pigs and sheep were measured using cylindrical punches (Gouldstone et al., 2003b).

††
Lungs of dogs, pigs and horses inflated at 4–16 cm H2O were measured using uniform pressure indentation, but only the data of dogs are presented here (Hajji et al., 1979).

†††
Cells from human alveolar and bronchial epithelial cell lines were measured using sharp pyramidal probes with semi-included angle 0=35° (Alcaraz et al., 2003).